Touchpoint-tailored ultrasensitive piezoresistive pressure sensors with a broad dynamic response range and low detection limit

Chen, Ming; Li, Kun; Cheng, Guanming; He, Ke; Li, Weiwei; Zhang, Daoshu; Li, Weimin; Feng, Ye; Wei, Lei; Li, Wenjie; Zhong, Guohua; Yang, Chunlei

2018

Chen, M., Li, K., Cheng, G., He, K., Li, W., Zhang, D., ... Yang, C. (2019). Touchpoint-tailored ultrasensitive piezoresistive pressure sensors with a broad dynamic response range and low detection limit. ACS Applied Materials & Interfaces, 11(2), 2551-2558. doi:10.1021/acsami.8b20284

https://hdl.handle.net/10356/143256

https://doi.org/10.1021/acsami.8b20284

Touchpoint-tailored ultra-sensitive piezoresistive pressure sensors with a broad dynamic response range and low detection limit

Abstract:

Wearable pressure sensors with high sensitivity, broad dynamic response range and low detection limit are highly desirable to enable the applications in electronic skins and soft robotics. In this work, we report a high-performance wearable pressure sensor based on microstructured polydimethylsiloxane (PDMS)/Ag and rough polyimide (PI)/Au interdigital electrodes. By tailoring the touchpoints, the resulting pressure sensors show ultrahigh sensitivity (259.32 kPa^{-1}), broad dynamic response range (54 kPa) and low detection limit (0.36 Pa). We also systematically investigate the effect of different sensor structural configurations, PDMS geometrical feature, and Ag thickness on the performance of the pressure sensors. Thanks to these merits, the fabricated pressure sensor is capable of real-time monitoring pulse wave, and can act as a part of the mechanical hand to detect weak pressure changes, leading to the great application promise in the fields of biomedical, real-time health monitoring and intelligent robot.

Keywords: piezoresistive, wearable pressure sensors, microstructures, touch points, motion sensor.

Introduction:

Flexible, wearable and lightweight pressure sensing devices are of paramount importance for various applications, such as soft robotics, health monitoring, and energy harvesting. To date, pressure sensors with different working mechanisms have been demonstrated, including capacitive, piezoelectric, triboelectric and resistive. Among which, the piezo-resistivity pressure sensors appear to be more promising due to their simplicity in device fabrication and high sensitivity, as well as relatively low energy consumption in operation [need some refs].

Under external pressure, the change of the electrical resistance is commonly due to the changes either in the material's microstructure or the contact resistance between two contacting electrodes. In the first case, various nanomaterials including nanowires, carbon nanotubes, polymer nanofibers, and graphene have been used to form the electrical percolation pathway. The change of the electrical resistance is mainly due to the breakup and reforming process of the electrical percolation pathways. In the latter case, the change of the contact resistance is mainly ascribed to the deformation of the elastic matrix. This kind of pressure sensor has been successfully applied for healthcare monitoring. Nevertheless, it is still challenging to fabricate flexible and wearable pressure sensors which can combine high sensitivity, large operating pressure range and low detection limit.

In most cases, the sensitivity ($(\Delta I/I_0)/\Delta P$) is defined as the ratio of current or resistance change with pressure, which is mainly caused by the variation of sensor contact area. Thus, the sensitivity is proportion to the variation of the contact area. On

the other hand, for the operating pressure range, larger structural variation process is expected for the pressure sensors to experience. The typical strategy to improve the performance is to introduce fine microstructure features on the surfaces of the contacting elastics electrodes. Compared to the pressure sensors with flat structures, this method enables a greater variation of contact area and more variation states. Surface textures of elastomers, for example, polydimethylsiloxane (PDMS) microstructures, are the common ways to form pressure sensors. Zhu et al reported a piezoresistive pressure sensor with pyramid PDMS microstructure/graphene film/ITO/PET configuration and demonstrated a high sensitivity of -5.53 kPa^{-1} within a pressure range from 0 to 100 Pa. Peng et al systemically studied the effects of PDMS geometrical features on the performance of the pressure sensors and found the micro-semicylinder-based sensor had the highest sensitivity of -3.6 kPa^{-1}. Recently, Wang et al found that the pressure sensors with irregular PDMS patterns (microhump patterns *via* sandpaper mold) showed higher sensitivity and broader operating pressure regime, comparing with regular micropatterned devices. However, most of the work focus on the design of the top PDMS microstructures. In principle, microstructures in both the top and bottom matrix will enhance the performance of the pressure sensors, as more variation of the contact area and larger structural variation process can be expected.

Herein, we propose and demonstrate a high performance pressure sensor by combing PDMS/Ag microstructures and rough PI/Au interdigital electrodes. Compared to the devices with flat bottom electrodes or flat top PDMS, the proposed configuration shows a significantly enhanced sensitivity. We also systemically investigate the

influence of top contact area, the thickness of Ag film, and the height of PDMS microstructures on the device performance. The resulting wearable sensor exhibites high sensitivity (259.3 kPa^{-1}), broad working range (54 kPa) and low detection limit (0.36 Pa). Meanwhile, the fabricated pressure sensor could be attached on human skin to monitor the real-time pulse wave. Furthermore, the pressure sensors can be integrated into an intelligent mechanical hand to detect the weak movement of a light-weight table tennis, demonstrating its high potential for application in soft robotics.

Results and discussion

Figure 1a schematically illustrates the key process steps for the fabrication of the PDMS/Ag/Au/PI pressure sensor. The top microstructures are transferred onto the flexible PDMS mold by simple lithography and casting process, followed by the deposition of Ag film. The PI/Au interdigital electrodes are prepared *via* electrochemical method with irregular patterns. Then, the device is formed by assembling PDMS/Ag and PI/Au interdigital electrode. Figure 1b-c and Figure S1 are the scanning electron microscopy (SEM) images of the resulting patterned PDMS mold with clearly defined conical frustum-like microstructures. Figure 1d-e depicts the corresponding atomic force microscope (AFM) images. The peak to peak roughness is ~300 nm. For the fabricated PI/Au interdigital electrodes, Figure 1f-g and Figure S2 show the corresponding SEM and AFM images, and the peak to peak roughness of the electroplated Au is ~1.4 μm. As a result, these hierarchical, conical frustum-like structured PDMS/Ag and electroplated PI/Au electrodes provide large surface area,

sufficient roughness and elasticity to “feel” the variation of contact resistance when the external pressure is loaded, which in principle can improve the sensitivity and enlarge the working range of the pressure sensor.

Figure 2a-b represent the assembled device. The formed pressure sensor shows good mechanical flexibility. To demonstrate the improved performance of the proposed structure, three types of pressure sensors including Flat-Rough structure, Rough-Flat structure (the peak-to-peak roughness of the fabricated smooth PI/Au interdigital electrode is ~180 nm, as shown in Figure S3), and Rough-Rough structure are designed and fabricated, as schematically illustrated in Figure 2c. The response performance of the pressure sensors with different configurations are investigated and plotted in Figure 2d. Here, ΔI is defined as I_P-I_0, where I_P is the measured current under loading and I_0 is the initial current of the sensor. The sensor sensitivity, $(\Delta I/I_0)/\Delta P$, can be obtained by the linear slope of the plot before the current saturation. Additionally, depending on the operating scopes, each current-pressure curve is divided into two-parts (low- and high-pressure ranges) and linearly fitted for evaluating the sensor performance. The measured sensitivity is 8.64 (0.0026) KPa^{-1}, 6.41 (0.025) KPa^{-1} and 259.32 (0.33) KPa^{-1} in the low (high)-pressure ranges for the sensors with Flat-Rough, Rough-Flat and Rough-Rough configurations, respectively. Compared with other two common configurations (Flat-Rough and Rough-Flat), the Rough-Rough configuration offers the highest sensitivity and the broadest working range. These results verify that microstructures in both the top and bottom matrix will largely enhance the performance of the pressure sensors. The cycling test of the Rough-Rough pressure sensor is also

investigated, as shown in Figure 2e, and the relative current changes remain about the same value after 1000 loading/unloading cycles, which indicates the high durability of the proposed Rough-Rough pressure sensor. This high durability is ascribed to the excellent elasticity of the PDMS microstructures which can endure many mechanical deformation cycles.

The reason for the significant improvement in the performance of the Rough-Rough pressure sensor is due to the fact that this configuration experiences more variation of the contact area and larger structural variation process. To be more specific, during the loading process, when the longest top microstructure touches the highest position of the interdigital electrode and form a conductive path, the current will increase significantly. With the continuous deformation of the longer microstructure, the current will gradually increase until another set of conducting paths is formed, for example, the conducting paths formed by shorter microstructures. In general, due to the rough top microstructures and rough interdigital electrode, compared to other two configurations, our fabricated pressure sensor experienced many states-several point contacts to simultaneous plenty of point contacts to surface contacts, which finally contributes to its ultrasensitive and wide range features.

As the contact area has a great influence on the performance of the pressure sensor, by adjusting the development time in the fabrication process, pressure sensors (Rough-Rough configuration) with different top contact areas are fabricated. The diameter of the top contact area is 1.6 μm, 2.7 μm, and 3.8 μm, respectively, as shown in Figure 3a-f. Its influence on the pressure response performance is plotted in Figure 3g. The

pressure sensor with larger top area shows superior performance in the sensitivity and working range. The observation of this performance difference can be well explained by the following equation:

$$R_C(P) = k((P + P_{in})A_C)^{-n} \quad (1)$$

where $R_C(P)$ is the contact resistance under the loading pressure P, P_{in} is the initial pressure, and A_C is the contact area. The values of k and n depend on the device characteristics. It is clear that the contact resistance decreases as the contact area increases. Under the same external loading pressure, with increasing the top area, the effective contact area between the top microstructures and bottom interdigital electrode increases, leading to a larger variety of resistance (R/R_0, where R is the measured resistance under loading and R_0 is the initial resistance of the sensor), which in turn contributes to the higher sensitivity. On the other hand, the volume of the top microstructures decreases as the top area decreases. The deformation of the microstructures with smaller top area will be larger when experiencing the same external pressure. In other words, the deformation become easier to saturate, which finally lead to the results that the pressure sensor with larger top area possesses wide response range and high sensitivity.

Ag conducting film, as a key component of the pressure sensor, plays an important role on the sensitivity. Here we fabricate four kinds of pressure sensors (Rough-Rough configuration), in which the only difference is the Ag thickness. The thickness influence on the pressure response performance is investigated and plotted in Figure 3h-i. The measured sensitivity is 0.33 (0.18) KPa^{-1}, 126.7 (0.61) KPa^{-1}, 184 (0.47) KPa^{-1} and

259.32 (0.33) KPa^{-1} in the low (high)-pressure range for the sensors with Ag thickness of 30 nm, 50 nm, 70 nm and 100 nm, respectively (The morphologies of these Ag films are shown in Figure S4). The present results have the following features. Firstly, the pressure sensor with 30-nm-thick Ag has the lowest sensitivity (both in low- and high-pressure ranges) and the narrowest work range. That is because the 30-nm-thick-Ag possesses the highest resistance (R_{film}) (See Figure 3j, ~35*10-8 Ω • m), and hence the highest contact resistance R_c, ($R_{film}>R_c$). That makes R_0/R ($(R_c+R_{film})/(R_c+R_{film}-\Delta R_c)$, $\Delta R_c<<R_{film}$) comparatively small, in other words, resulting in a low value of $\Delta I/I_0$ and narrow work range. Secondly, the pressure sensor with 100-nm-think-Ag possesses the highest sensitivity in the low-pressure range, this is due to the decrement of R_c+R_{film} as a function of the thickness of Ag film. Thus, a high value of R_0/R ($\Delta I/I_0$) is obtained. Thirdly, the pressure sensor with 50-nm-thick-Ag possesses the highest sensitivity in the high-pressure range. We believe this is caused by the relatively small value of I_0 for the case with 50-nm-thick-Ag film, as the current change ΔI resulting from the deformation of PDMS microstructure is comparatively high, which in return contributes to high value of $((\Delta I/ I_0)/P)$ in the high-pressure range.

Our Rough-Rough pressure sensor is also quite sensitive for the detection of weak pressure changes. Figure 4a-b shows the response of the pressure sensor upon loading/unloading the rice with different weight. The high sensitivity and fast response time indicate that the resulting sensor is very suitable for detecting low pressure. Specially, the detection limit of our pressure sensor is only 0.32 Pa, this is by far the lowest detection limit (See Table 1 in the supporting information). We attribute this

result to the ultrahigh sensitivity property of the pressure sensor in the low-pressure region (increment of point contacts). Figure 4c displays the case of using the proposed pressure sensor as a pulse detector. As can be seen from Figure 4d, the electrical signal is stable, and we can clearly find several important peaks of the human pulse waveform, namely, P-wave (percussion), T-wave (tidal) and D-wave (diastolic) peaks.

A wearable and soft skin with the capability of sensing force, pressure, and temperature is one of the most important components of an intelligent robot. As a proof of concept, we design the following experiments. We first mounte a mechanical hand on the stepping motor and the fabricated Rough-Rough pressure sensor is conformally wrapped at the fingertips of this mechanical hand, as shown in Figure 4e. The mechanical hand moves forward the table tennis at a constant speed. When the pressure sensor touches the edge of a table tennis, the current increase rapidly. We set a threshold current for the stepping motor. When the output current reaches the threshold current, the stepping motor will move in the opposite directions (see the movie 1). Figure 4f shows the response curves of the fabricated pressure sensor to the mechanical hand movements. It can be seen from the peaks that the resistance decreases immediately and quickly recovers. In addition, the repeatability is pretty good, which again demonstrates that the proposed Rough-Rough pressure sensor possesses low pressure detection limit and high sensitivity. Our pressure sensors hold great application promise in the fields of medical health, wearable electronic devices, and intelligent robot development.

Conclusion

In summary, we develop a resistive wearable pressure sensor based on PDMS/Ag microstructures and rough PI/Au interdigital electrodes. The resulting pressure sensors exhibit high sensitivity (259.3 kPa^{-1}), wide working range (54 kPa), and low detection limit (0.36 Pa). Furthermore, the pressure sensor can act as a part of human skin for the real-time monitoring the human pulse wave, and can be integrated into an intelligent mechanical hand to detect the slight swing of a table tennis. These remarkable features of our pressure sensors offer great potential for biomedical, energy harvesting, and intelligent robot applications.

Experimental Section

Characterization and Performance Testing: For AFM measurement, Agilent 5500 was used. For SEM measurements, ZEISS SUPPA 55 equipped with Oxford EDS detector was used. For Ag resistance measurement, four-point probe instrument was used. The testing system is shown in Figure S5. The current-voltage (I-V) characteristics of the pressure sensors were determined using a semiconductor parameter analyzer (Keithley, 2400).

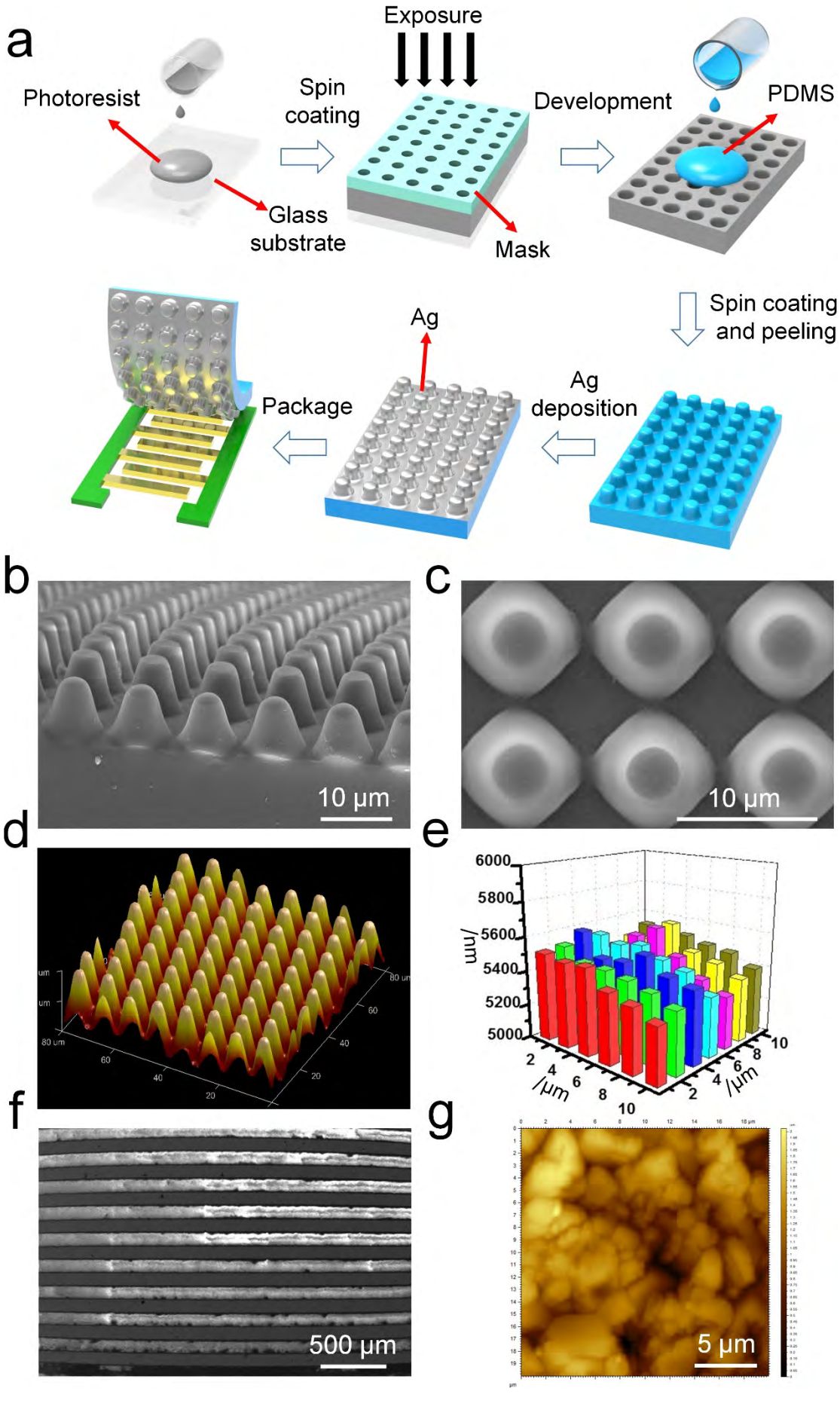
a
Photoresist
Glass substrate
Spin coating
Exposure
Mask
Development
PDMS
Spin coating and peeling
Ag deposition
Ag
Package
b
10 μm
c
10 μm
d
e
6000
5800
5600
5400
5200
5000
/nm
/μm
/μm
f
500 μm
g
5 μm

Figure 1 | Rough-Rough pressure sensors. a, Schematic illustration of the fabrication process of the Rough-Rough pressure sensors. **b-c,** Cross-sectional and top-view SEM images of the conical frustum-like PDMS microstructures. **d-e**, 3D surface morphologies and height profile of the conical frustum-like PDMS microstructures. **f-g,** SEM and AFM images of the rough electroplated PI/Au interdigital electrodes.

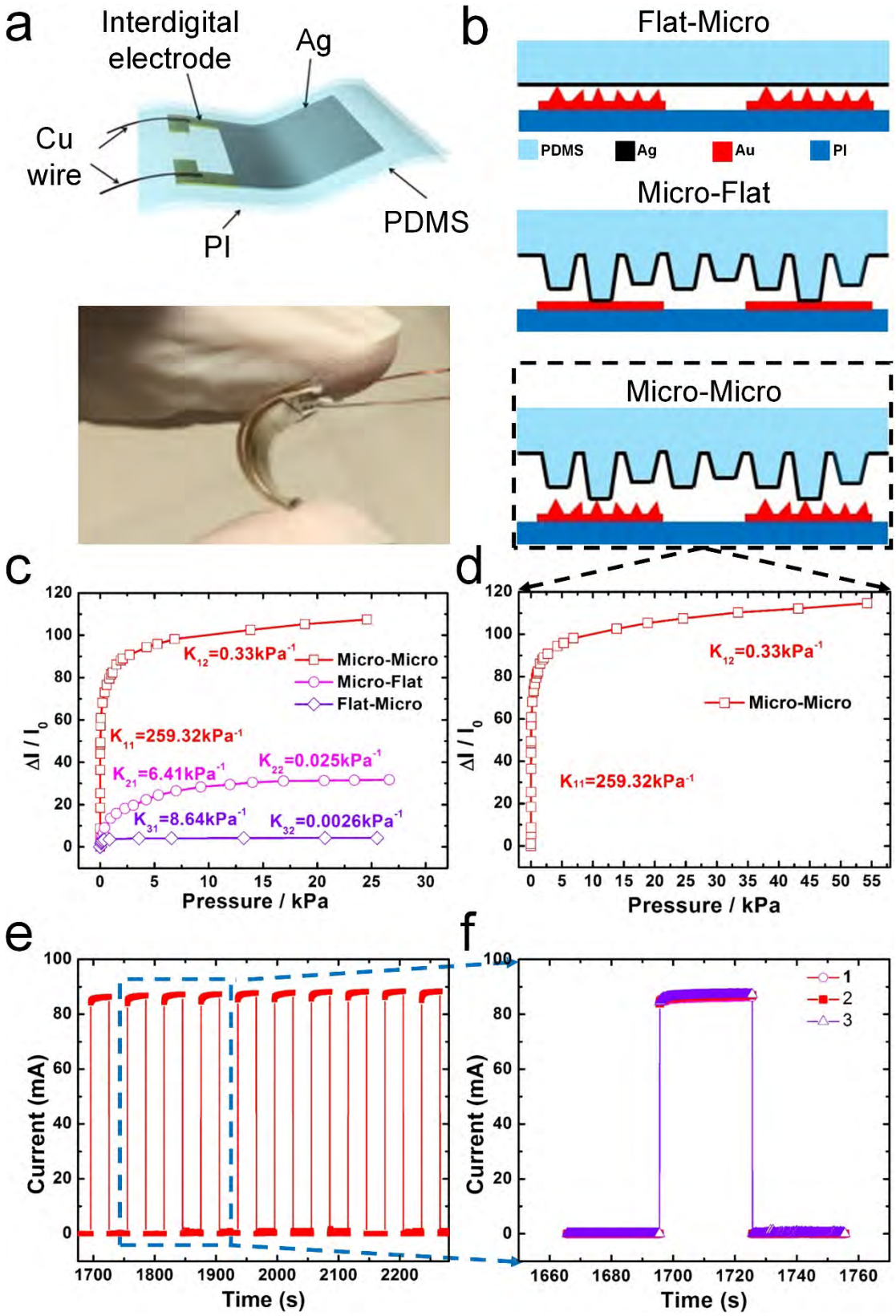

Figure 2 | Pressure-sensing capabilities of the microstructured pressure sensors. a, Schematic of the assembled Rough-Rough pressure sensor. **b,** Photograph of a bent Rough-Rough pressure sensor, indicating the well mechanical flexibility. **c,** The

diagram of three different sensor structures. **d,** The comparison of pressure sensitivities of different sensor structures: Rough-Rough structure (red), Rough-Flat structure (magenta), Flat-Rough structure (purple). **e**, Real-time I-t curves of the Rough-Rough pressure sensor for more than 1000 loading/unloading cycles with an applied pressure of 0.47 KPa.

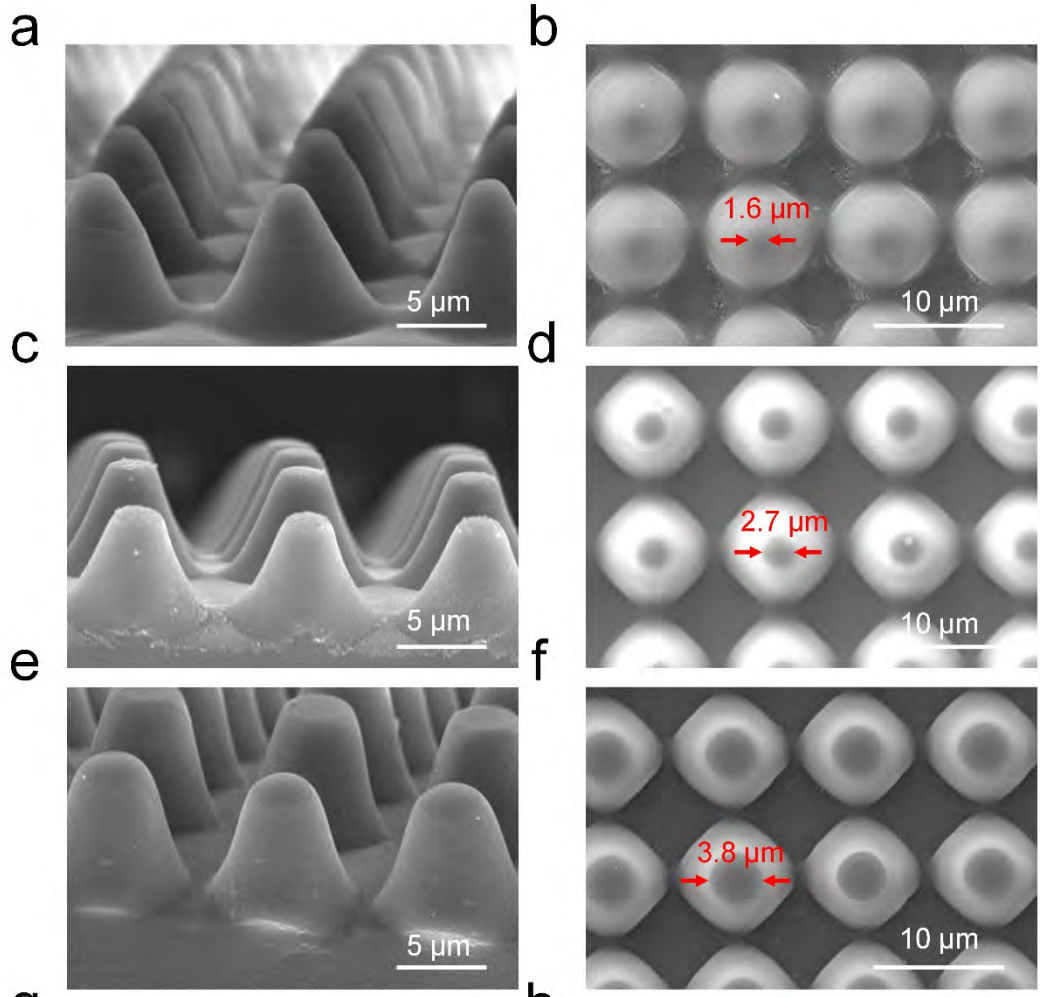
a
5 μm
b
1.6 μm
10 μm
c
5 μm
d
2.7 μm
10 μm
e
5 μm
f
3.8 μm
10 μm

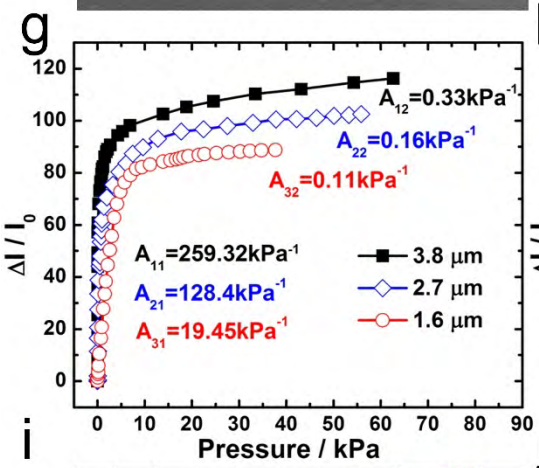
g
A12=0.33kPa-1
A22=0.16kPa-1
A32=0.11kPa-1
A11=259.32kPa-1
A21=128.4kPa-1
A31=19.45kPa-1
3.8 μm
2.7 μm
1.6 μm
ΔI / I0
Pressure / kPa

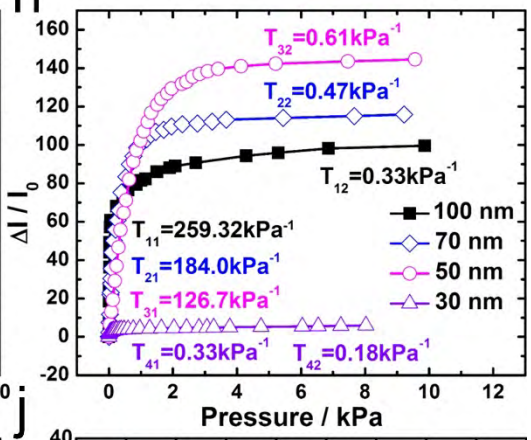
h
T32=0.61kPa-1
T22=0.47kPa-1
T12=0.33kPa-1
T11=259.32kPa-1
T21=184.0kPa-1
T31=126.7kPa-1
T41=0.33kPa-1
T42=0.18kPa-1
100 nm
70 nm
50 nm
30 nm
ΔI / I0
Pressure / kPa

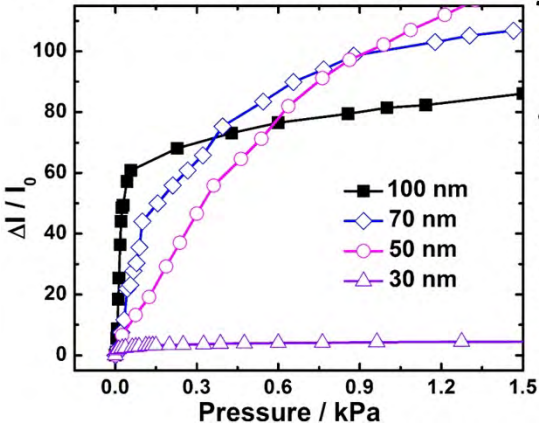
i
100 nm
70 nm
50 nm
30 nm
ΔI / I0
Pressure / kPa

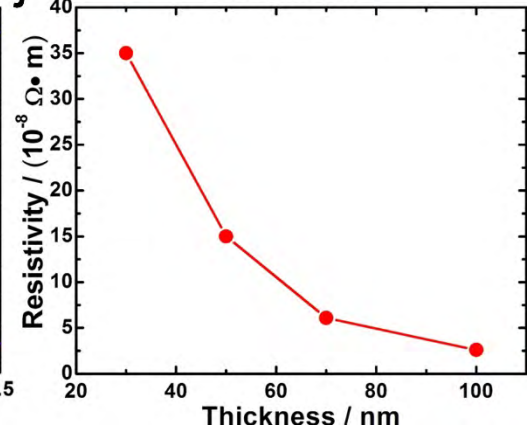
j
Resistivity / (10-8 Ω• m)
Thickness / nm

Figure 3 | Pressure-sensing capabilities of the microstructured pressure sensors. a-f, SEM images of Rough-Rough pressure sensors with different top contact areas. The diameter (D) of the top contact area are 1.6 μm, 2.7 μm, and 3.8 μm, respectively. **a** and **c** and **e** are the cross-sectional SEM images; b and d and f are the top-view SEM images. **g,** The comparison of pressure sensitivities of the Rough-Rough sensors with different top contact areas: D = 1.6 μm (red), D = 2.7 μm (blue), D = 3.8 μm (black). **h**, The comparison of pressure sensitivities of the Rough-Rough sensors with different Ag thicknesses (0 - 10 kPa). **i**, The comparison of pressure sensitivities of the Rough-Rough sensors with different Ag thickness (0 - 1.5 kPa). **j**, The resistivity of Ag film as a function of thickness.

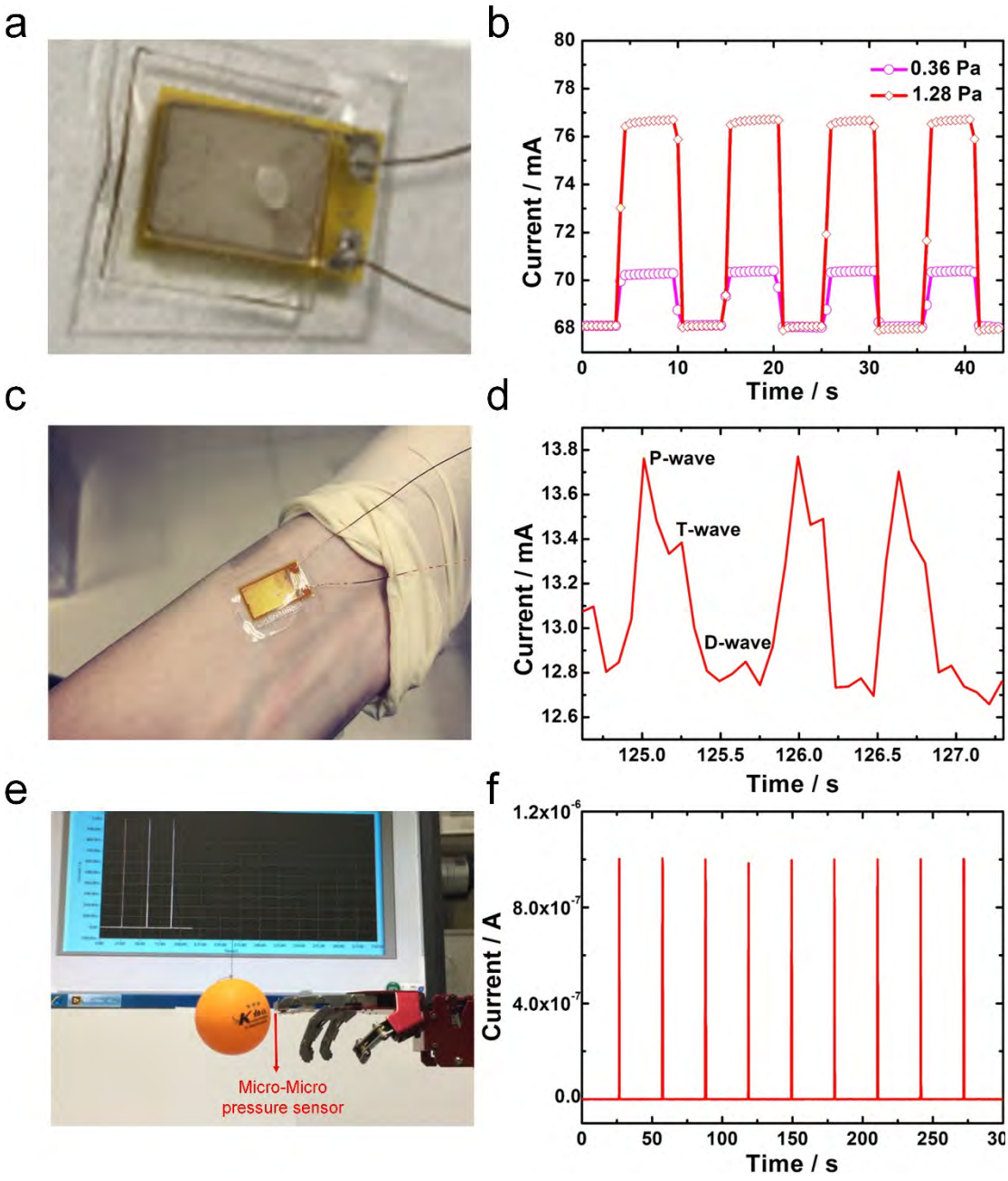

Figure 4 | Applications of the Rough-Rough pressure sensors. a-b, Detection of weak pressure: Optical image and current curve of the proposed Rough-Rough pressure sensor pressed by a rice grain. Weak pressures can be detected by the proposed pressure sensors, and the detection limit reaches 0.36 Pa. **c-d,** Real-time health monitoring: the detection of wrist pulses by the Rough-Rough pressure sensor attached on the wrist. **e-f**, Intelligent robots: optical image and current curve of the proposed Rough-Rough pressure sensor pressed by a suspended table tennis (4g). The curves in f indicate the low detection limit and high response speed merits of our pressure sensors.